Improving the detection sensitivity of gravitational wave searches in non-stationary data

Jiayu Wang,[1] Ajit Kumar Mehta,[1] and Tejaswi Venumadhav[1,2]

[1] *Department of Physics, University of California at Santa Barbara, Santa Barbara, CA 93106, USA*
[2] *International Centre for Theoretical Sciences, Tata Institute of Fundamental Research, Bangalore 560089, India*

(Dated: February 2, 2025)

A key factor influencing detection sensitivity of gravitational wave search pipelines is "non-stationarity" of the LIGO detector data, where the noise power spectral density (PSD) varies over time [1–3]. Previous studies have addressed the leading-order effects of PSD variation on the search background, assuming that PSD drifts are independent of frequency bins [3, 4]. These leading order considerations were shown to improve the detection sensitivity by $\sim 10\%$. In this paper, we extend this analysis by developing a method that accounts for the frequency dependence of PSD drifts. Applying this method to LIGO data, we demonstrate that accounting for frequency-dependent PSD variations could further enhance the detection volume by $\sim 2\% - 6\%$ depending on the number of frequency bands used in the analysis.

I. INTRODUCTION

The LIGO and Virgo detectors are now routinely detecting gravitational wave (GW) signals from the mergers of compact binary systems. The observations thus far [5–7] have already provided unprecedented insights into the nature of compact objects and strong field gravity [8–11]. The detection process relies on the matched-filtering technique, where the detector's strain data are cross-correlated with theoretical GW templates to identify signals buried in noise. This method is most effective under the assumption that the noise is stationary and follows a Gaussian distribution.

However, it is well-established that the noise in GW detectors is generally non-stationary. The non-stationary behavior can be distinguished into two types. The first one is the non-Gaussian noise transients that produce a high signal-to-noise ratio (SNR). (known as "glitches" on a sub-second timescale). These glitches may be caused by the environment, such as seismic noise, or instrumental malfunction[12, 13]. The second type of noise is caused by a longer time-scale variation ($\sim 10s$) of the power spectral density (PSD)[1–3]. For the first type of noise, `PyCBC` analysis employs a signal consistency test[14]. Here we focus on resolving the second type of noise. If these variations are not adequately taken into account, they can result in a reduction in detector sensitivity of more than $\sim 10\%$. In existing GW search pipelines, such as `IAS` [2, 15], `Gstlal` [16], and `PyCBC` [6], this effect has been addressed typically assuming that the changes (or drifts) in the PSD are independent of frequency components [3, 4].

In this paper, we relax the assumption that PSD drifts are independent of frequency bins (or bands) and instead explore their frequency dependence. We derive a corrected detection statistic that incorporates this effect, which we refer to as the *band drift corrected overlap*. The analysis with band drift-corrected SNR involves dividing the matched-filtering overlaps into $n_{\rm band}$ disjoint frequency bands such that each band contributes equally to the optimal SNR of the injected GW signals [17]. Within each frequency bins, we estimate the PSD drift statistics using method desribed in [3]. For comparison, we retain the *scalar drift corrected overlap*, which assumes frequency-independent PSD drifts. We evaluate the performance of these corrected statistics by applying them to artificially injected GW signals in randomly selected Hanford detector data spanning one week from the second part of the third observing run (O3b). Since we are focusing on the second type of noise, we mitigate the effect of the loud noise transients with a χ^2 test in the `PyCBC` search pipeline which down-ranks these glitches[17].

Our analysis demonstrates that the scalar drift correction improves the detection sensitivity of the LIGO detectors by $\sim 10\%$ for long-duration signals ($\gg 1$ second) and $\sim 2\%$ for short-duration signals ($\lesssim 1$ second). These results are broadly consistent with previous studies [3, 4]. On the other hand, we show that applying band drift corrections can provide an additional improvement in detection sensitivity of $\sim 2\% - 6\%$, largely independent of the morphology of the GW signals. We find that improvements remain similar up to $n_{\rm band} = 10$ frequency bands, the maximum number of bands we investigated in this work.

The remainder of this paper is organized as follows: Section II introduces the PSD drift-corrected detection statistics used in this work, with a full derivation of the band drift-corrected matched-filter statistic provided in Appendix A. Section III details the injection setup and presents the results of applying the corrected detection statistics to artificially injected GW signals in O3b data. Finally, Section IV concludes the paper and discusses potential future directions. All analyses presented in this paper were performed using the `PyCBC` software package [18].

II. NEW DETECTION STATISTIC

If the noise is stationary and Gaussian, the optimal detection statistic is $|z|^2$, where z is the matched-filter overlap defined as,

$$z(t_0) = \langle d(t), \hat{h}(t; t_0)\rangle \tag{1}$$

with

$$\hat{h} = \frac{h}{\sqrt{\langle h, h\rangle}} \tag{2}$$

where $d(t)$ represents the strain data, and $h(t; t_0)$ is the GW signal template for a compact binary system with coalescence time t_0 (the time of merger). Here, t_0 is varied to obtain the overlap time-series $z(t_0)$. The term $\langle h, h\rangle$ is referred to as the optimal signal-to-noise ratio (SNR) of the signal h. The inner product $\langle ., .\rangle$ is defined as

$$\langle a, b(t_0)\rangle = 2\int_{-\infty}^{\infty} \frac{\tilde{a}(f)\tilde{b}^{\star}(f)}{S_n(f)}\, e^{2\pi i f t_0} df \tag{3}$$

where $S_n(f)$ denotes the PSD of the noise (see Eq. 5 below), tilde ($\sim$) indicates the Fourier transform and star ($\star$) denotes the complex conjugation.

The PSD of the noise is estimated directly from LIGO data using the standard Welch 's method. [19] In this method, the data is divided into multiple segments (which may overlap or not), and each segment is processed using a window function, followed by a discrete Fourier transform (DFT). The PSD, $S_n(f)$, is then computed as the median of the power spectra obtained from all segments. The number and duration of the segments are determined based on the required frequency resolution and precision of the PSD measurement. As demonstrated in [3], to limit detection sensitivity loss to a few percent, the PSD for LIGO data typically needs to be measured over a duration of approximately 10^3 seconds. [1]

To assess the applicability of the matched-filtering overlaps (z) for detecting GW signals, it is essential to first examine the underlying assumption that whether the data is stationary. Ref. [3] addressed this by computing the variance of z for a single template on the second observing run (O2) data. To do this, they averaged the power (z^2) within rolling windows of ~ 15 seconds (see Fig. 1 therein). Ideally, this should result in a stochastic measurement error of $\sim 2\%$. However, Fig. 1 clearly shows deviations from unity (expected under a Gaussian distribution) of $\sim 8\% - 10\%$. The authors attributed this discrepancy to the non-stationarity of the data, which manifests on timescales as short as tens of seconds (see Fig. 2 therein). This effect leads to mis-estimation of the PSD, thereby affecting the variances of z. Below, we provide a more detailed explanation of this effect.

Borrowing the notations from Ref. [3], the autocorrelation function of the data is expressed as:

$$\langle d(T - \tau/2), d(T + \tau/2)\rangle = C_n(\tau) + \delta C_n(\tau; T) \tag{4}$$

where $C_n(\tau)$ represents represents the stationary component of the data, depending only on the lag τ, and decaying exponentially for large τ. The two-sided PSD is defined as the FT of $c_n(\tau)$ as

$$S_{n,2}(f) = \int_{-\infty}^{\infty} d\tau\, C_n(\tau)\, e^{2\pi i f\tau} \tag{5}$$

One-sided PSD ($S_n(f)$) is defined as half of the two-sided PSD ($S_{n,2}(f)$) for $f \in [0, \infty)$ as $C_n(\tau)$ is real-valued for the real-valued data $d(t)$. The term $\delta C_n(\tau; T)$ accounts for deviations from stationarity and is time-dependent. We write it in the frequency domain as:

$$\epsilon(f; T) = \frac{1}{S_{n,2}(f)} \int_{-\infty}^{\infty} d\tau\, \delta C_n(\tau; T)\, e^{2\pi i f\tau} \tag{6}$$

such that the time-dependent PSD can be expressed as:

$$S_{n,2}(f; T) = S_{n,2}(f)[1 + \epsilon(f; T)] \tag{7}$$

Here, $\epsilon(f; T)$ quantifies the fractional change in the PSD at a frequency f over a slowly varying time $T \gg \tau$. Note that τ is conjugate to f.

A. Matched-filter overlaps with scalar drift correction

To simplify the problem, we first assume that the PSD drifts are independent of frequency, varying uniformly across all frequencies. In this case, the PSD is expressed as $S_{n,2}(f; T) = S_{n,2}(f)[1 + \epsilon(T)] \equiv \alpha(T) S_{n,2}(f)$, where we call $\alpha(T)$ as the scalar drifts. Based on this, we define a corrected matched-filter overlap:

$$z_s(t) = \frac{z(t)}{\sqrt{\alpha(t)}} \tag{8}$$

where $\alpha(t)$ is an estimate of the scalar drift at time t. This definition ensures that the variance of z_s is unity at all times t.

An estimator for $\alpha(t)$ is provided in Appendix B of Ref. [3]. and in Ref [4]. However, their result indicates that instead of $z(t)\alpha(t)^{-\kappa}$, which $\kappa = 0.5$, in this case, estimates of $\kappa \gtrsim 0.33$ are obtained. Thus, in Ref[20], a corrected statistic of $z(t)\alpha(t)^{-0.33}$ was applied to the search pipeline. Here we are using the estimator provided by [3] and using $\kappa = -0.5$

B. Matched-filter overlaps with band drift correction

In the general case where PSD drifts vary with frequency, we write our corrected matched-filter overlap as follows:

$$z_b(t) = \sum_{f_n} \frac{z_n(t)}{\sqrt{\alpha_n(t)}} \tag{9}$$

where f_n with $n = 1, 2, ..., n_{\rm band}$, denotes discrete frequency bands whose union covers the frequency range of interest. The parameters α_n are determined by requiring that the variance of z_b is unity and that the corrected SNR is maximized at each time. The detailed derivation is provided in Appendix A. We find:

$$\sqrt{\alpha_n} = \sigma_n^2 \sqrt{\sum_{f_n} \frac{1}{\sigma_n^2}} \tag{10}$$

Here, σ_n^2 is the variance of the matched-filter overlaps $z_n(t)$ within the frequency band f_n. Eq. 10 holds when the frequency bands are chosen such that each band contributes equally to the optimal SNR of the template $h(t)$, a criterion adopted in this work. For computational efficiency, we use $n_{\rm band} = 4$ as the default value for the results presented in this work; however, we will later discuss how the results are affected by varying $n_{\rm band}$.

C. χ^2-veto corrected statistic

In this work, our aim is to understand the impact of the non-stationarity in LIGO data on detection sensitivity. However, LIGO data is also subject to non-Gaussianities, which manifest as short-duration disturbances, also known as "glitches". These glitches can mimic real signals, complicating the analysis. To mitigate this, GW search pipelines such as `PyCBC` employ a χ^2-veto test. This test examines whether the time-frequency power distribution in the data is consistent with the expected power distribution of the template waveform [17, 21]. With this test, the detection statistic presented in Eq. 1 is modified as [4]:

$$\hat{z} = \begin{cases} z, & \chi_r^2 \leq 1 \\ z\left[\frac{1}{2}(1 + (\chi_r^2)^3)\right]^{-1/6}, & \chi_r^2 > 1 \end{cases} \tag{11}$$

Incorporating non-stationarity into this framework, we define the scalar drift-corrected statistic as:

$$\hat{z}_s = \begin{cases} \hat{z}_s, & \chi_r^2 v_s^{-1} \leq 1 \\ z\left[\frac{1}{2}(v_s^3 + (\chi_r^2)^3)\right]^{-1/6}, & \chi_r^2 v_s^{-1} > 1 \end{cases} \tag{12}$$

and for the band drift-corrected statistic as:

$$\hat{z}_b = \begin{cases} \hat{z}_b, & \chi_r^2 v_b^{-1} \leq 1 \\ z\left[\frac{1}{2}(v_b^3 + (\chi_r^2)^3)\right]^{-1/6}, & \chi_r^2 v_b^{-1} > 1 \end{cases} \tag{13}$$

Here, χ_r^2 is the chi-squared test statistic for a given trigger, $v_s = \alpha$ is the scalar drift, and v_b is the band drift correction, defined as:

$$v_b = \left(\frac{z}{\hat{z}_b}\right)^2 \tag{14}$$

We refer to $|\hat{z}_s|^2$ and $|\hat{z}_b|^2$ as our final detection statistics for scalar drift and band drift corrections, respectively.

D. Performance of the corrected detection statistics

We evaluate the performance of the different detection statistics defined in Eqs. 1, 8, 9, 11, 12, and 13 by analyzing multiple strain files randomly selected from the full O3b run of the Hanford detector, corresponding to approximately one week of data. The squared values of these detection statistics are presented in Fig. 1.

The χ^2-veto is observed to significantly reduce trigger rates at high detection statistic values, irrespective of the signal duration. This is expected, as high detection statistic values are often associated with glitches. Additionally, the PSD drift-corrections further suppress trigger rates at high detection statistic values for long-duration signals (see the upper panel of Fig. 1). However, for short-duration signals (e.g., $\lesssim 1$ seconds, shown in the lower panel), PSD drift corrections do not result in a significant difference in trigger rates between the detection statistics. This suggests that PSD drift corrections can improve the detection sensitivities of LIGO detectors for long-duration signals. However, this improvement may not be guaranteed, as the corrected matched-filter SNRs of astrophysical signals could also be affected.

To confirm any potential improvement, an injection study is necessary. This involves injecting artificially generated astrophysical signals into the data and comparing their detection statistic values against the background. Such a study would enable precise estimation of any enhancement in the detection sensitivity volume. We discuss this in more detail below.

III. IMPROVEMENT IN THE DETECTION SENSITIVITY

A. Injections

We simulate GW signals emitted by binary black hole (BBH) systems with component masses and spins as specified in Table I. The chosen mass range would capture the effects of PSD drifts on both long-duration and short-duration GW signals within the detector's sensitivity band. We consider two cases for the dimensionless spin components perpendicular to the orbital plane: $\chi_{\rm eff} = -0.5\,\&\,0.5$,, where $\chi_{\rm eff}$ is the effective spin parameter of the binary system. Other parameters, such as sky location and inclination angle, are fixed to fiducial values across all the injections to compute the resulting strain signals.

The simulated strains are injected into Hanford detector data spanning roughly one week of observation time. The strains are scaled to have an optimal SNR of 4, calculated using the median PSD estimated from 200 Hanford data files from the O3b run. This SNR threshold focuses the analysis on signals near the detection limit, providing a better test of the detection statistic's sensitivity. The Hanford detector data is chosen for this study because

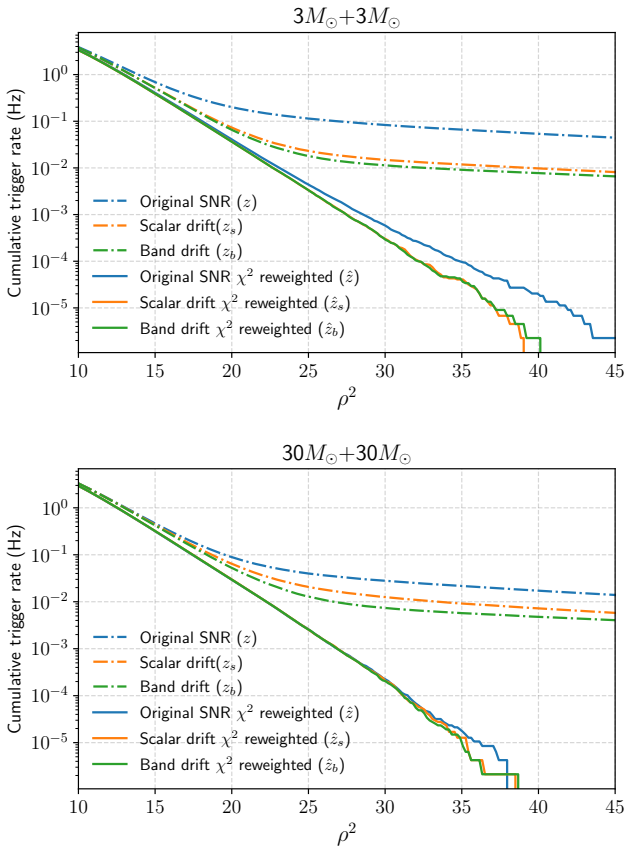

FIG. 1: The cumulative trigger rates for the χ^2- veto corrected detection statistics−namely, the original matched-filter overlap ($\hat{z}$), the scalar drift corrected overlap ($\hat{z}_s$) and the band drift corrected overlap ($\hat{z}_b$)−are shown for one week of Hanford strain data randomly selected from the O3b run. The *upper panel* shows the cumulative trigger distribution for a long-duration signal (a $3M_\odot + 3M_\odot$ BBH system with $\chi_{\rm eff} = 0.5$) while the *lower panel* shows the same for a short-duration signal (a $30M_\odot + 30M_\odot$ BBH system with $\chi_{\rm eff} = 0.5$).

m_1	m_2	$\chi_{\rm eff}$	SNR
$3M_\odot$	$3M_\odot$	0.5	4
$3M_\odot$	$3M_\odot$	-0.5	4
$30M_\odot$	$30M_\odot$	0.5	4
$30M_\odot$	$30M_\odot$	-0.5	4

TABLE I: Parameters of the injection signals; $m_{1,2}$ denote the component masses and $\chi_{\rm eff}$ represents the effective spin parameter. The last column lists the optimal SNR of the injection signal. The SNR is computed using a median PSD estimated from 200 randomly selected Hanford strain files of the O3b run.

it exhibits greater sensitivity to data quality issues compared to the Livingston detector. For each parameter configuration listed in Table I, we inject around 60,000 signals into the one-week observation data of O3b run.

Triggers are generated using all the detection statistics discussed so far. However, in the subsequent analysis, we focus exclusively on the results obtained with the χ^2- corrected detection statistics. For each injected signal, the detection statistic values are recorded as the maximum within a 0.1-second window centered on the merger (or peak) time of the signal. This time window is consistent with real GW searches, CITE where exact merger times are not known a priori. A similar analysis is performed on the background data (i.e., data without injected signals) to evaluate the false alarm rates (FARs) of the detected signals.

B. Results

In Fig. 2, we present the improvement in detection volume achieved when using the scalar and band drift-corrected overlaps (Eq.12) as detection statistics, compared to the original overlap (Eq.11). The shaded regions represent the error bars associated with the measurement of the detection volume gain (see Appendix B for details). The figure illustrates the fractional improvements for two binary systems: $m_1 = m_2 = 3M_\odot$ (long duration) and $m_1 = m_2 = 30M_\odot$ (short duration) with $\chi_{\rm eff} = 0.5$. In Fig. 4, we show the same for $\chi_{\rm eff} = -0.5$.

The results demonstrate that PSD drift corrections significantly enhance the detection sensitivity of LIGO detectors for long-duration signals, particularly at very low FARs. However, it is important to note that at lower FARs, the spacetime volume to which the detectors are sensitive also decreases. To address this, we adopt a conservative FAR threshold of 1 per 13 minutes for our detectability criteria in a single detector, following the approach in Ref. [4]. This threshold corresponds to a FAR of approximately 1 per year for the Hanford-Livingston detector network.

At this FAR threshold, scalar drift corrections improve the detection volume for long-duration signals by $7\% - 15\%$, depending on the binary's spin. Interestingly, negatively spinning binaries exhibit better performance with PSD drift corrections. For short-duration signals, the improvement is negligible for $\chi_{\rm eff} = 0.5$, with error bars encompassing zero, while for $\chi_{\rm eff} = -0.5$, the improvement could reach $\sim 1\%$ or slightly higher. This behavior is expected, as long-duration signals have extended integration times, making them more susceptible to PSD variations.

In contrast, band drift corrections provide more substantial improvements, with detection volume gains of $\sim 12\% - 20\%$ for long-duration signals. For short-duration signals, the improvement is also significant, averaging $\sim 3\% - 7\%$. These findings clearly demonstrate that band drift corrections outperform scalar drift corrections. This is further highlighted in the right panels of Figs. 2 and 4, where the band drift-corrected SNR is shown to be at least 2% more sensitive than the scalar drift-corrected SNR, with potential gains of up to $\sim 6\%$. Interestingly, the relative improvement provided by band

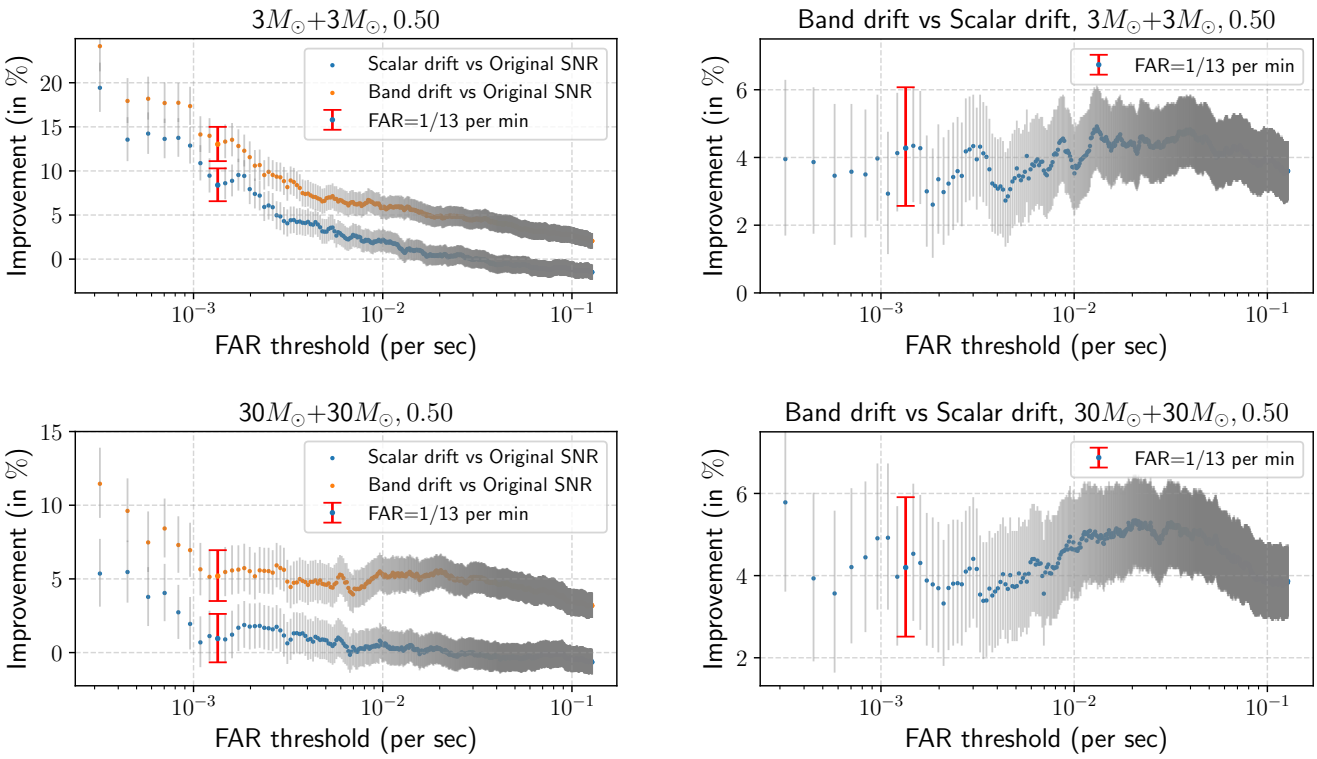

FIG. 2: *Left panel*: Improvement in the detection volume achieved with the scalar drift-corrected overlap ($\hat{z}_s$) and band drift-corrected overlap ($\hat{z}_b$) relative to the original matched-filter overlap (or SNR) without any PSD drift correction ($\hat{z}$), for binary systems with $m_{1,z} = 3M_\odot$, $m_{1,z} = 3M_\odot$ (*top plot*) and $m_{1,z} = 30M_\odot$, $m_{1,z} = 30M_\odot$ (*bottom plot*) at $\chi_{\rm eff} = 0.5$. The signals were injected at an SNR of 4 into approximately one week of O3b LVK data. *Right panel*: Relative improvement in the detection volume of the band drift-corrected overlap ($\hat{z}_b$) compared to the scalar drift-corrected overlap ($\hat{z}_s$) for the same binary configurations. The shaded regions around the points in each panel represent the error bars on the volume measurements. The error bars highlighted in red indicate results at a specific FAR of 1 per 13 minutes.

drift corrections appears to be largely independent of signal duration and morphology.

Dependency on $n_{\rm band}$: Fig. 3 illustrates the variation in volume improvement due to band drift corrections relative to scalar drift corrections at the chosen FAR of 1 per 13 minutes as a function of the number of frequency bands $n_{\rm band}$, for the $m_{1,z} = 3M_\odot$, $m_{1,z} = 3M_\odot$, $\chi_{\rm eff} = 0.5$ binary system. While the mean values of volume improvement increase with the $n_{\rm band}$ used, the overlapping error bars indicate that the differences are not statistically significant. Therefore, the results presented in this work should remain similar if a value of $n_{\rm band}$ other than 4 were chosen. In future work, we aim to employ singular value decomposition (SVD) to identify the optimal number of frequency bands that capture the most significant information while maintaining or enhancing detection sensitivity.

IV. CONCLUSION

In this work, we developed a method to account for the effects of frequency-dependent PSD variations on the standard detection statistic used to identify GW signals in LIGO data. The resulting statistic, referred to as the *band drift-corrected overlap*, generalizes the *scalar drift-corrected overlap*, which assumes frequency-independent PSD variations. While scalar drift corrections have already been implemented in GW search pipelines such as `IAS` and `PyCBC`, we demonstrated that incorporating band drift corrections can provide an additional improvement of $2\% - 6\%$ in the detection volume for GW signals. Accounting for frequency dependent non-stationary noise may be an important factor in the next generation of GW detectors with a higher bandwodth.

It is important to note that our current results are conservative estimates, as the analysis was performed using only four specific configurations of binary black hole (BBH) systems: $3M_\odot + 3M_\odot$ with $\chi_{\rm eff} = \pm 0.5$ and $3M_\odot$+$3M_\odot$ with $\chi_{\rm eff} = \pm 0.5$ These signals were injected into one week of O3b data from the Hanford detector to validate our method.

Future work will involve integrating the method developed here into the state-of-the-art `IAS` GW search pipeline [15, 22]. This will enable a comprehensive analysis of the entire O3b dataset from both LIGO detectors,

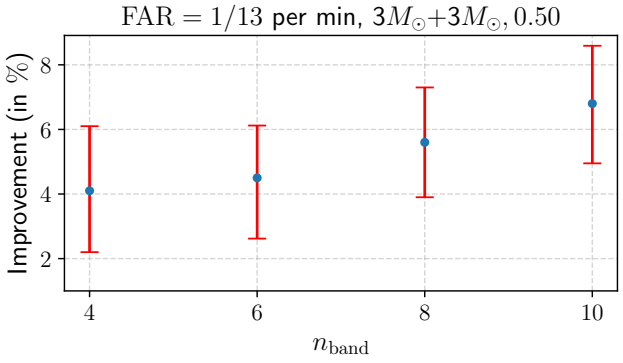

FIG. 3: Improvement in the detection volume achieved with the band drift-corrected detection statistic relative to the scalar drift-corrected detection statistic, evaluated at a FAR of 1 per 13 minutes. The results are shown for the binary system with $m_{1,z} = 3M_\odot$, $m_{1,z} = 3M_\odot$ and $\chi_{\rm eff} = 0.5$, as a function of the number of frequency bands ($n_{\rm band}$) used in the band drift correction.

with GW signals injected using an astrophysically motivated distribution of BBH parameters. This approach will allow us to robustly quantify the benefits of band drift corrections across a broader range of GW signal morphologies and astrophysical scenarios.

ACKNOWLEDGMENTS

We thank Sumit Kumar for providing help with the PyCBC search pipeline. We also thank Barak Zackay, Jaiver Roulet, Digvijay Wadekar and Matias Zaldarriaga for helpful discussions. TV acknowledges support from....[fill in the details here].

This research has made use of data, software and/or web tools obtained from the Gravitational Wave Open Science Center (https://www.gw-openscience.org/), a service of LIGO Laboratory, the LIGO Scientific Collaboration and the Virgo Collaboration. LIGO Laboratory and Advanced LIGO are funded by the United States National Science Foundation (NSF) as well as the Science and Technology Facilities Council (STFC) of the United Kingdom, the Max-Planck-Society (MPS), and the State of Niedersachsen/Germany for support of the construction of Advanced LIGO and construction and operation of the GEO600 detector. Additional support for Advanced LIGO was provided by the Australian Research Council. Virgo is funded, through the European Gravitational Observatory (EGO), by the French Centre National de Recherche Scientifique (CNRS), the Italian Istituto Nazionale di Fisica Nucleare (INFN) and the Dutch Nikhef, with contributions by institutions from Belgium, Germany, Greece, Hungary, Ireland, Japan, Monaco, Poland, Portugal, Spain.

Appendix A: Derivation of band drift corrected matched-filter statistic

Starting from Eq. 9, where the PSD drifts are not assumed to be independent across frequency bands, the band drift-corrected matched-filter overlap is expressed as:

$$z_b(t) = \sum_{f_n} \frac{z_n(t)}{\sqrt{\alpha_n(t)}} \tag{A1}$$

where f_n represents disjoint frequency bands whose union covers the full frequency range of interest. Our goal is to compute the PSD drift corrections, α_n, for each band such that the corrected SNR:

$$\rho_{\rm corr} = \frac{\langle |z_b| \rangle |_{h\neq 0}}{\sigma_z^2|_{h=0}} \tag{A2}$$

is maximized while ensuring that the variance ($\sigma^2_{z_b}$) remains unity at any given time t. Here, $h \neq 0$ corresponds to the hypothesis that the data $d(t)$ contains a signal $h(t)$ while $h = 0$ represents the null hypothesis (i.e., no signal is present). We perform this optimization using the method of Lagrange multiplier.

The Lagrangian is,

$$\mathcal{L}(\alpha, \xi) = f(\alpha) - \xi g(\alpha) \tag{A3}$$

where $\alpha = (\alpha_1, \alpha_2, ..., \alpha_n)$, ξ is the Lagrange multiplier, $f(\alpha) = \rho_{\rm corr}(\alpha)$ is the function to be maximized, and the constraint equation is given by,

$$g(\alpha) = \sigma^2_{z_b}(\alpha) - 1 = 0 \tag{A4}$$

Using Eq. A1, the corrected SNR can be written as

$$\rho_{\rm corr} = \sum_{f_n} \frac{\langle |z_n| \rangle |_{h\neq 0}}{\sqrt{\alpha_n}} \tag{A5}$$

and the variance is,

$$\sigma^2_{z_b} == \sum_{f_n} \frac{\sigma_n^2}{\alpha_n} \tag{A6}$$

where σ_n^2 is the variance of the matched-filter overlaps within the $n-th$ frequency band f_n. These expressions assume that the frequency bands are uncorrelated and that the mean $\langle z_n \rangle$ is zero under null hypothesis. (justify these assumptions!)

The condition for optimization with respect to the parameter α_n is given by,

$$\frac{\partial f(\alpha)}{\partial \alpha_n} = \xi \frac{\partial g(\alpha)}{\partial \alpha_n} \tag{A7}$$

Solving this yields,

$$\alpha_n = \frac{4\sigma_n^4 \xi^2}{\mu_n^2} \tag{A8}$$

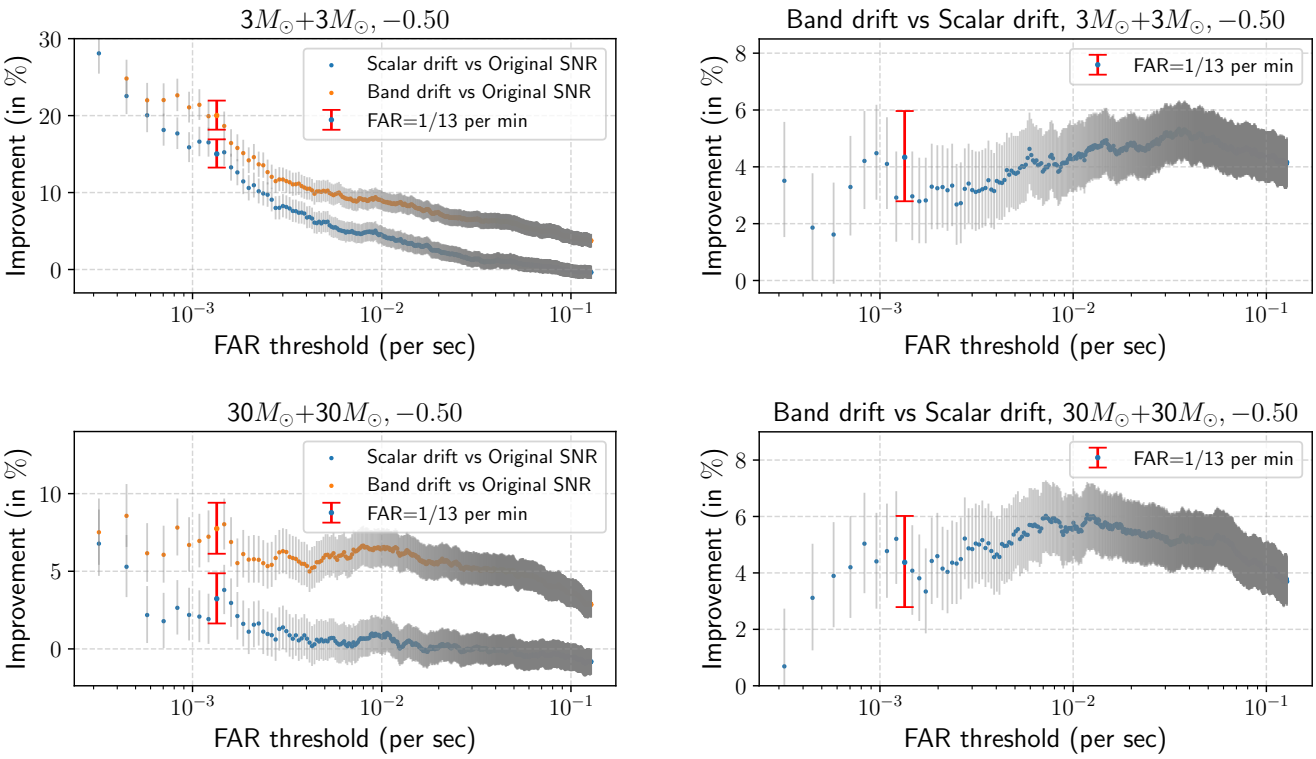

FIG. 4: Same as Fig. 2 but with the effective spin, $\chi_{\rm eff} = -0.5$.

where $\mu_n = \langle |z_n| \rangle |_{h \neq 0}$ is the fraction of the optimal SNR of the template h within the frequency band f_n.

Using the constraint Eq. A4, we find,

$$\xi^2 = \sum_{f_n} \frac{1}{4\sigma_n^2 \mu_n^2} \tag{A9}$$

Substituting this back into Eq. A8 gives,

$$\alpha_n = \frac{\sigma_n^4}{\mu_n^2} \sum_{f_n} \frac{1}{\sigma_n^2 \mu_n^2} \tag{A10}$$

If we choose frequency bands f_n such that the contributions to the optimal SNR (μ_n) are equal, the PSD drift correction simplifies to:

$$\sqrt{\alpha_n} = \sigma_n^2 \sqrt{\sum_{f_n} \frac{1}{\sigma_n^2}} \tag{A11}$$

Appendix B: Estimation of the measurement error

Our aim in this work is to measure the gain in the detection volume-time (if any) achieved through band drift corrections to the PSD, compared to scalar drift corrections. To quantify this, we define:

$$\lambda = \frac{\overline{VT}_j - \overline{VT}_i}{\overline{VT}_i} \tag{B1}$$

where $\overline{VT}_i$ represents the detection volume-time for the $i-th$ detection statistic, as defined in Eqns. 11, 12 and 13. The parameter λ therefore quantifies the fractional improvement in the detection volume-time of the $j-th$ detection statistic relative to the $i-th$ detection statistic.

Let us consider the case where we detect n_i and n_j events using detection statistics i and j respectively, at a given FAR, from an analysis of one week of O3b data. Let us assume that n_i follows a Poisson distribution with the average number of detections given by $R_0 \overline{VT}_i$, where R_0 is the local merger rate density of compact binary systems of interest. Consequently, the probabilities of observing n_i and n_j detections are given by:

$$P(n_i|\overline{VT}_i, R_0) = \frac{e^{-R_0 \overline{VT}_i} (R_0 \overline{VT}_i)^{n_i}}{n_i!} \tag{B2}$$

and,

$$P(n_j|\overline{VT}_j, R_0) = \frac{e^{-R_0 \overline{VT}_j} (R_0 \overline{VT}_j)^{n_j}}{n_j!} \tag{B3}$$

Let us denote $\mu \equiv \overline{VT}_i$. Using Bayes's theorem,

$$P(\mu, \lambda|n_i, n_j, R_0) = \frac{P(n_i, n_j|\mu, \lambda, R_0)\, P(\mu, \lambda|R_0)}{P(n_i, n_j|R_0)} \tag{B4}$$

where:

$$P(n_i, n_j|\mu, \lambda, R_0) \propto e^{-R_0 \mu (2+\lambda)}\, \mu^{n_i+n_j}\, (1+\lambda)^{n_j} \tag{B5}$$

and,

$$P(\mu, \lambda|R_0) = P(\mu|\lambda, R_0)\, P(\lambda|R_0) \tag{B6}$$

Let us marginalize over μ. The posterior for λ becomes:

$$P(\lambda|n_i, n_j, R_0) \propto \int d\mu \left[e^{-R_0\mu(2+\lambda)}\, \mu^{n_i+n_j}\, (1+\lambda)^{n_j} \times P(\mu|\lambda, R_0)\right] \times P(\lambda|R_0) \tag{B7}$$

We finally obtain,

$$P(\lambda|n_i, n_j, R_0) = \text{Constant} \times \frac{(1+\lambda)^{\mathrm{n_j}}}{(2+\lambda)^{\mathrm{n_i}+\mathrm{n_j}+1}} \times \mathrm{P}(\lambda|\mathrm{R_0}) \tag{B8}$$

Assuming a uniform prior for $P(\lambda|R_0)$ over a sufficiently wide range of λ, the posterior $P(\lambda|n_i, n_j, R_0)$ provides the distribution of λ for given values of n_i and n_j detections. In this work, we compute the 68% symmetric credible interval around the maximum of the posterior, $P(\lambda|n_i, n_j, R_0)$ to report the uncertainty in the measurement of λ.

[1] B. P. Abbott *et al.*, Classical and Quantum Gravity **37**, 055002 (2020).
[2] T. Venumadhav, B. Zackay, J. Roulet, L. Dai, and M. Zaldarriaga, Phys. Rev. D **100**, 023011 (2019), arXiv:1902.10341 [astro-ph.IM].
[3] B. Zackay, T. Venumadhav, J. Roulet, L. Dai, and M. Zaldarriaga, Phys. Rev. D **104**, 063034 (2021).
[4] S. Mozzon, L. K. Nuttall, A. Lundgren, T. Dent, S. Kumar, and A. H. Nitz, Classical and Quantum Gravity **37**, 215014 (2020), arXiv:2002.09407 [astro-ph.IM].
[5] R. Abbott *et al.* (LIGO Scientific, VIRGO, KAGRA), (2021), arXiv:2111.03606 [gr-qc].
[6] A. H. Nitz, S. Kumar, Y.-F. Wang, S. Kastha, *et al.*, Astrophys. J. **946**, 59 (2023), arXiv:2112.06878 [astro-ph.HE].
[7] D. Wadekar, J. Roulet, T. Venumadhav, A. K. Mehta, *et al.*, (2023), arXiv:2312.06631 [gr-qc].
[8] R. Abbott *et al.* (LIGO Scientific, VIRGO, KAGRA), (2021), arXiv:2112.06861 [gr-qc].
[9] R. Abbott *et al.* (KAGRA, VIRGO, LIGO Scientific), Phys. Rev. X **13**, 011048 (2023), arXiv:2111.03634 [astro-ph.HE].
[10] J. Roulet, T. Venumadhav, B. Zackay, L. Dai, and M. Zaldarriaga, Phys. Rev. D **102**, 123022 (2020), arXiv:2008.07014 [astro-ph.HE].
[11] R. Abbott *et al.* (LIGO Scientific, KAGRA, VIRGO), Astrophys. J. **970**, 191 (2024), arXiv:2304.08393 [gr-qc].
[12] B. P. Abbott *et al.*, Classical and Quantum Gravity **33**, 134001 (2016).
[13] L. K. N. et al, Classical and Quantum Gravity **32**, 245005 (2015).
[14] B. Allen, W. G. Anderson, P. R. Brady, D. A. Brown, and J. D. E. Creighton, Phys. Rev. D **85**, 122006 (2012).
[15] D. Wadekar *et al.*, in preparation (2023).
[16] S. Sachdev, S. Caudill, H. Fong, R. K. L. Lo, *et al.*, (2019), arXiv:1901.08580v1 [gr-qc].
[17] B. Allen, Phys. Rev. D **71**, 062001 (2005), arXiv:gr-qc/0405045.
[18] "v2.3.3 release of PyCBC," `https://zenodo.org/badge/latestdoi/31596861` (Published January 9, 2024).
[19] P. Welch, IEEE Transactions on audio and electroacoustics **15**, 70 (1967).
[20] A. H. Nitz, T. Dent, G. S. Davies, S. Kumar, *et al.*, Astrophys. J. **891**, 123 (2020), arXiv:1910.05331 [astro-ph.HE].
[21] S. A. Usman *et al.*, Class. Quant. Grav. **33**, 215004 (2016), arXiv:1508.02357 [gr-qc].
[22] D. Wadekar, J. Roulet, T. Venumadhav, A. K. Mehta, *et al.*, arXiv e-prints , arXiv:2312.06631 (2023), arXiv:2312.06631 [gr-qc].